Nanoscopic interchain aggregate domain formation in conjugated polymer films studied by third harmonic generation near-field scanning optical microscopy

Richard D. Schaller, Preston T. Snee, Justin C. Johnson, Lynn F. Lee, Kevin R. Wilson, Louis H. Haber, and Richard J. Saykally[a]
Department of Chemistry, University of California, Berkeley, Berkeley, California 94720-1460

Thuc-Quyen Nguyen[b] and Benjamin J. Schwartz[c]
Department of Chemistry and Biochemistry, University of California, Los Angeles, Los Angeles, California 90095-1569

The electronic structure of conjugated polymer films is of current interest due to the wide range of potential applications for such materials in optoelectronic devices. A central outstanding issue is the significance of interchain electronic species in films of these materials. In this paper, we investigate the nature of interchain species in films of poly[2-methoxy-5-(2′-ethylhexyloxy)-1,4-phenylene vinylene] (MEH-PPV) both before and after thermal annealing. Our investigation employs a combination of third harmonic generation (THG) and near-field scanning optical microscopy to measure the wavelength and spatial dependence of the THG efficiency. These chemically selective imaging measurements reveal new, low-energy absorption features in nanometer-scale spatially distinct regions of annealed films that are only infrequently observed prior to annealing. This suggests that the polymer strands in annealed MEH-PPV films pack together closely enough that significant ground-state wave function overlap can occur: thermal annealing creates nanoscopic aggregation domains. THG polarization studies indicate that polymer chain segments in these domains have a preferred orientational alignment. The spatial correlation of these aligned nanoscopic regions within the annealed films suggests that they form via a nucleation and growth type mechanism. In combination with previous work, these data support the idea that the nature and spatial distribution of interchain interactions in conjugated polymer films are complex; conjugated polymer films likely contain an inhomogeneous spatial distribution of both ground- and excited-state interchain species. © *2002 American Institute of Physics.*
[DOI: 10.1063/1.1499479]

I. INTRODUCTION

Conjugated polymers present many potential optoelectronic applications, including use in devices such as light-emitting diodes (LEDs),[1–4] photodiodes,[5] photovoltaics,[6] and large-area displays.[7,8] The optimization of such devices has been hindered, however, due to uncertainty regarding the electronic properties of the polymer strands when they are cast into films. Mounting evidence indicates that interchain species significantly influence the electronic properties of films of these materials.[9–16] Not only can such interchain species be detrimental to device efficiency due to their low-emission quantum yields,[13,17,18] but they may also be important in device degradation due to their long excited-state lifetimes and position as the lowest-energy species in energy funneling processes.[19] Thus, understanding both the details of the electronic interactions between conjugated polymer chromophores and the way chromophore interactions are dis-

tributed spatially throughout conjugated polymer films is critical if these materials are to be exploited to their maximum potential.

Despite their importance, interchain electronic species in conjugated polymers are difficult to study because the way in which the conjugated chromophores interact depends sensitively on the how the conjugated polymer film was processed.[9,10,20,21] In conjugated polymer films produced by spin-coating, for example, the rapid evaporation of the solvent results in films in which the polymer chains are kinetically frozen into a wide variety of conformations that may or may not foster interchain species. Thermal annealing of a conjugated polymer film, in contrast, allows the individual polymer strands to explore configuration space and results in chains that are packed in a more thermodynamically favorable fashion, thus increasing the interactions between adjacent polymer chromophores.[10,12,22–25] In both as-cast and annealed conjugated polymer films, a balance between the steric repulsion of bulky side chains and maximization of π-electron delocalization also can result in domains of molecularly oriented polymer chromophores,[26–31] as well as interchain delocalized ground and/or excited electronic states.[10,12–14,32] While several groups have observed submi-

cron scale orientation domains in films of conjugated polymers using near-field scanning optical microscopy (NSOM) techniques,[26,28,30,31,33–35] relatively little has been learned regarding the spatial distribution of interchain electronic species in these materials.

The primary spectral signature of interchain excited states is the presence of a weak, redshifted photoluminescence (PL), which has a radiative lifetime that is much longer than the emission from a single polymer chain.[13,14,17,32,36–39] Many experiments have also found evidence for intermolecular ground-state species, or "aggregates," which are characterized by the presence of a weak, redshifted feature in the absorption spectrum of the polymer in addition to the weak redshifted interchain PL.[26,27,40–43] Throughout this paper, we will take care to distinguish the interchain electronic species that form when a conjugated polymer chromophore is in its excited state, such as "excimers"[14,16,18,37] or "polaron pairs,"[14,15,32,44–46] from those interchain species that form when the π electrons are delocalized between chromophores in the ground electronic state, such as aggregates.[10,26,27,40–43] We also make a point to differentiate interchain electronic species from orientation domains; even if polymer strands are aligned due to physical or chemical interactions, this does not necessarily result in overlap of ground-state wave functions between chromophores.

Third-harmonic generation (THG) is a powerful spectroscopic method for the study of ground-state electronic species; it is a parametric process and therefore does not depend on the particular relaxation channels (either radiative or nonradiative) of the excited state.[47–49] This sensitivity to ground-state electronic properties allows us to use THG to distinguish ground-state species such as aggregates, which may or may not be emissive, from excited-state interchain species, such as excimers and polaron pairs, which are characterized only by their PL. The combination of THG with NSOM allows a sample to be imaged in a manner similar to that of linear absorption but without the high background levels associated with transmission spectroscopies.[50,51] The THG signal is proportional to the third-order polarizability, $P_i^{(3)}$, induced in a sample, as described by the equation[47,48]

$$P_i^{(3)}(3\omega) \propto \chi_{ijkl}^{(3)} E(\omega_j) E(\omega_k) E(\omega_l), \tag{1}$$

where $\chi_{ijkl}^{(3)}$ is a fourth-rank tensor that describes the coupling of the three electric fields, $E(\omega_{j,k,l})$, to create the third-harmonic polarization, and i, j, k, and l are electric field orientations with respect to laboratory coordinates. $\chi^{(3)}$ consists of both nonresonant and resonant terms

$$\chi_{\text{total}}^{(3)} = \chi_{\text{NR}}^{(3)} + \chi_{\text{R}}^{(3)}, \tag{2}$$

where the resonant term $(\chi_{\text{R}}^{(3)})$ can be described more explicitly as

$$
\begin{aligned}
&\chi_{ijkl}^{(3)}(-3\omega, \omega, \omega, \omega) \\
&\approx \sum_{n,n',n'' \neq g} \frac{\langle g|i|n \rangle}{(3\omega - \omega_{ng} + i\Gamma_{ng})} \\
&\times \frac{\langle n|l|n'' \rangle \langle n''|k|n' \rangle \langle n'|j|g \rangle + \text{permutations}}{(2\omega - \omega_{n''g} + i\Gamma_{n''g})(\omega - \omega_{n'g} + i\Gamma_{n'g})}
\end{aligned}
\tag{3}
$$

and can increase THG signals by orders of magnitude when the experimental frequencies ω, 2ω, 3ω (or combinations of them) approach the frequencies of molecular transitions ω_{ng}, $\omega_{n'g}$, and $\omega_{n''g}$ in the sample. The transition dipole matrix elements $\langle g|i|n \rangle$ represent the coupling between the ground state g and an excited state n along the i coordinate. Γ is a characteristic damping constant for the corresponding molecular transitions. We have recently shown that the combination of resonantly enhanced nonlinear optical processes and NSOM is useful for subwavelength spatial resolution imaging with chemical specificity.[50–54] For THG NSOM, the fact that a third-order polarization can be generated in centrosymmetric media provides sensitivity to the bulk of the sample, in contrast to the surface selectivity that can be engendered via second-order nonlinear optical processes, such as second-harmonic or sum frequency generation.[47]

Several groups have used THG (although not THG NSOM) to investigate the electronic properties of conjugated polymers. Saito and co-workers studied the THG of highly oriented Langmuir–Blodgett films of a dialkoxy-derivitized poly(phenylene vinylene) (PPV) and found a strong dependence of the THG efficiency on the incident laser polarization.[55] The data from these experiments showed that the THG signals were ~15 times stronger when the incident laser polarization was parallel to the orientation of the polymer backbone than when the laser polarization was perpendicular to the polymer backbone direction. This result confirms that the most important component of the third-order polarizability tensor that leads to the THG response is $\alpha_{\zeta\zeta\zeta\zeta}^{(3)}$ (where ζ is the direction along the polymer backbone and $\chi_{ijkl}^{(3)}$ is proportional to $\alpha_{\zeta\zeta\zeta\zeta}^{(3)}$), as others have previously assumed.[56,57] In addition to the work by Saito and co-workers, both Mathy et al.[58] and Yang et al.[59] have shown that three-photon resonant THG measurements on conjugated polymers closely reproduce the linear absorption spectra of polymer samples; the only deviation noted was a slight variation in intensity near the absorption maximum that was attributed to resonance with vibronic states of the exciton. These workers also found that at wavelengths for which the resonant enhancement is not changing rapidly, $\chi^{(3)}$ is proportional to L_d^6, where L_d is the delocalization length of a one-dimensional polymer. We note that Ledoux and co-workers have shown in THG studies of long chain polyenes that L_d does not continuously increase but instead is known to saturate.[60]

In this study, we use THG NSOM to investigate both as-cast and thermally annealed films of poly[2-methoxy-5-(2′-ethylhexyloxy)-1,4-phenylene vinylene] (MEH-PPV), with the goal of quantifying the significance and spatial distribution of ground electronic state interchain species. As mentioned above, THG is sensitive to the absorp

tive properties of chromophores in a sample. This allows us to discriminate between aggregation in the ground state and the presence of interchain species such as excimers that form only in the excited state, even if both aggregates and excimers produce a similar interchain emission. The expected spectral signature of ground-state interchain species is an absorption spectrum that is shifted to the red of the single-chain absorption, a result of the additional delocalization of the π-electrons between the polymer chains. This provides a clear spectral window in which to observe the presence of conjugated polymer aggregates via THG. The low-background nature of THG is critical to the success of these measurements: aggregate absorption is usually too weak to be observed in transmission, and the fact that aggregate emission is strongly quenched in films[13,14,32,61] makes it difficult to observe the aggregate absorption using photoluminescence excitation.[10] In addition, the long excited-state lifetime of interchain species [small value of Γ in Eq. (3)] should greatly increase the resonant enhancement produced by any interchain species, providing strong signals even with the possibility of small values of $\langle g|i|n\rangle$.

In the results that follow, we present evidence that nanoscopic, prolate-shaped ($\sim 600 \times 200$ nm on average) domains of ground-state interchain species exist with high frequency in annealed films of MEH-PPV but are only rarely present in as-cast films. THG NSOM images produced on resonance with the single-chain absorption in annealed films result in stronger THG signals, but do not show any image contrast. However, ''aggregation'' domains are observed in THG NSOM images when the third-harmonic energy is tuned to the red of the lowest-energy single-chain absorption frequency. The aggregation domains exhibit increased THG efficiency further to the red than film regions that do not appear to contain aggregate domains. We also find that aggregation domains are rare in as-cast (nonannealed) films; the few domains that are observed, however, are associated with topographical bumps on the surface of the film. This is consistent with a picture that aggregates, which form infrequently in solution, can survive spin casting and persist into the film, a process also associated with the choice of casting solvent.[10,40] THG NSOM polarization studies reveal that the nanoscopic aggregation domains show orientation and thus may be associated with previously observed orientation domains in MEH-PPV films.[30,31] An analysis of the spatial correlation between aggregation domains indicates that these domains may form according to a nucleation and growth mechanism during the thermal annealing process. All the results argue that conjugated polymer films have a processing-history-dependent complexity to the presence and spatial distribution of interchain species that must be understood in order to fully exploit these materials for applications.

II. EXPERIMENT

A commercial (TMmicroscopes, Lumina) shear-force feedback-mechanism-equipped NSOM system, which has been described previously,[12,52,53,62,63] was used for near-field measurements of THG signals. Fiber optic probes were chemically etched to a ~ 50 nm diameter tip and were not metal coated. We have previously demonstrated an optical
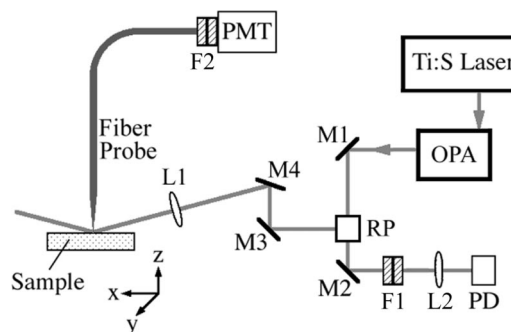

FIG. 1. THG NSOM experimental setup. Optical parametric amplifier (OPA); steering mirrors (M1–4); Rochon prism (RP); filters (F1–2); Ge photodiode (PD). Signal and idler wavelengths produced in the OPA were separated by the RP. Idler wavelengths (1.60–2.70 μm) were used to produce the third harmonic while the signal wavelengths (1.16–1.60 μm) were monitored with the PD to normalize for shot to shot laser fluctuations. THG signals collected by the near-field probe were directed to filters and a photomultiplier tube (PMT) detector that could be replaced with a 0.3 m monochrometer and back-illuminated, liquid-nitrogen-cooled CCD to check that unwanted three-photon-induced PL was not a significant component of the THG signals.

spatial resolution of 108 nm using these uncoated fibers in similar nonlinear NSOM studies.[51,63] Optical and topographical data were obtained simultaneously for comparison. Forward and reverse motions of the sample were used to produce separate images of the sample as a check of image reproducibility. Repeatable optical images were then averaged together to reduce noise.

The light source for the experiments consisted of a home-built titanium:sapphire oscillator (800 nm, 480 mW, 30 fs, 88 MHz), which was used to seed a commercial (Spectra-Physics) chirped pulse amplifier (800 nm, 2.25 W, 80 fs, 1 kHz). The output of the amplifier pumped a commercial (Quantronix, Topaz) superfluorescence optical parametric amplifier (OPA) to generate tunable femtosecond pulses in the near-ir (1.16–2.7 μm, 300 μJ at 1350 nm, 80 fs). As shown in Fig. 1, the signal and idler pulses emerging from the OPA were separated using a calcite Rochon prism. A Ge photodiode and boxcar integrator were used to monitor the intensity of the signal pulses for normalization. The idler pulses were passed through a 1.5 μm long-pass filter to remove any residual visible light. The intensity of the idler pulses was attenuated using a stepped neutral density filter and were subsequently focused onto the sample at 60° from normal incidence to a ~ 100 μm diameter spot with p polarization (except where noted) at the position where the probe investigated the sample. As with our previous work on these samples,[12,64] special measures were taken to prevent photo-oxidative damage to the sample in these experiments. All optical measurements were performed under a nitrogen-purged atmosphere and the incident average laser power was maintained at ~ 700 μW for all laser frequencies. For the NSOM images displayed below, each pixel represents the average of 46 laser shots, and the images are 200×200 pixel arrays. Complete images required ~ 30 min to collect, and no image processing was performed except where explicitly noted. THG spectral data points for fixed positions on the sample represent the average of 12 000 laser shots.

Dispersion of the optical signals collected by the NSOM

tip with a spectrograph and charge-coupled device (CCD) camera indicate that three-photon PL could be produced when the incident beam was on resonance, but that the relative integrated intensity of this light is quite small (<2% of the THG signal).

MEH-PPV samples were prepared in the same manner as in our previous emission studies of these films.[10,12,64] The polymer solutions and films were prepared in an inert N_2 atmosphere. MEH-PPV was dissolved in chlorobenzene in the dark for several hours to give 1% (w/v) solutions. The polymer solutions were spin-cast onto acid-cleaned glass substrates and the resulting ~200 nm thick films were heated at 50 °C for several hours to evaporate any residual solvent. Annealed films were produced by heating above the glass transition temperature of the polymer [~205 °C for our polymer with molecular weight ~1×10^6 g/mol (Ref. 10)] for several hours in a nitrogen glovebox.

III. RESULTS AND DISCUSSION

A. Background: Spectral signature of interchain species in conjugated polymers

Much of the work on interchain species in conjugated polymers has focused on MEH-PPV.[9–15,20,32,36,37,39,40,44,65–68] Single-molecule experiments have shown that the conformation and electronic properties of individual MEH-PPV chains can be controlled by the processing conditions.[19,61,67,68] For bulk MEH-PPV samples, it has been argued that memory of the polymer conformation and degree of aggregation in solution is preserved through the spin-casting process and persists in the film.[10,12] This memory is manifested by topographical bumps on the surface of spin-cast films that vary in both size and frequency depending on the solvent and concentration of the solution from which the film was cast. Furthermore, PL NSOM experiments conducted on as-cast films show that the topographic bumps frequently exhibit a broad, redshifted PL spectra compared to topographically flat regions of the film, indicating that the bumps correspond to regions containing a higher concentration of emissive interchain species.[12]

The broad, redshifted emission from the topographic bumps in as-cast MEH-PPV films is quite similar to the emission from thermally annealed films, in which the electronic structure of the entire film is comprised predominantly of interchain species. Thermally annealed films have a smooth topography on the nanometer scale, consistent with the idea that the more freely flowing chains in the polymer melt can pack into thermodynamically favorable lower-energy structures.[10] NSOM experiments have found negligible spatial variation in the PL of annealed films, indicating that the distribution of emissive species is highly homogeneous[12] (although spatial variation in the PL is observed when high-polarity liquids are applied to the film surface, indicating that different emissive excited-state interchain species with a variety of dipole moments exist in thermally annealed MEH-PPV films).[64] The annealing process also causes a change in the uv–visible absorption spectrum:[30] the red onset of the main low-energy absorption feature shifts further to the red upon annealing. The shift of the absorption to redder wavelengths is indicative of an overall increase in electron delocalization that can be realized by two different means. First, annealing may reduce the number of kinks in single polymer chains, resulting in increased π-electron delocalization along *individual* chains. Second, annealing may cause multiple polymer chains to pack tightly together, allowing for *interchain* π-electron delocalization. The fact that the spectral signatures of interchain species (a weak redshifted absorption and even weaker redshifted emission) are so subtle is what makes them difficult to study, even if they are present in high concentrations in annealed conjugated polymer films. One of the goals of this study is to use NSOM-based spectroscopic methods to image the spatial distribution of interchain species in annealed conjugated polymer films.

Other groups also have employed NSOM to investigate the properties of conjugated polymer films. In work by Blatchford *et al.*,[26] ~200 nm diameter orientation domains in films of poly (*p*-pyridyl vinylene) (PPyV) were observed using polarization modulation (PM) transmission and polarized PL NSOM, techniques that can provide insight into the variation of average orientation of absorption and emission transition dipoles. No correlation was found between the presence of these domains and the film surface topography, indicating that the orientation domains were present in the bulk of the film. Buratto and co-workers studied the electronic properties of stretch-oriented PPV films using PL[33] and photoconductivity[34,69] NSOM. Credo *et al.*[70] as well as McNeill *et al.*[71] have studied carrier mobility in MEH-PPV films using photo-oxidation and electric-field-modulated PL NSOM, respectively. Teetsov and Vanden Bout used PL NSOM to observe ordered domains in annealed thin films of 9,9-dialkylpolyfluorenes[28,29] that exhibited high polarization ratios. Fann and co-workers also have employed PM NSOM and have observed orientation domains in films of PPV[31] and MEH-PPV[30] that were on the order of hundreds of nanometers in spatial extent. We note again, however, that the observation of orientation domains in all of these studies does not necessarily implicate the existence of domains of interchain aggregation. All of these results could be explained by the presence of domains of aligned, individual polymer chains without the need to invoke the concept of interchain electronic structures in these regions. In particular, the transmission measurements in Refs. 30 and 31 were conducted at wavelengths that are primarily absorbed by single-chain species, leaving open the question of whether or not the aligned domains are comprised of interchain species. The weak, redshifted absorption features characteristic of interchain species are difficult to observe in transmission, and the reduced PL quantum efficiency of aggregated domains in films makes them equally difficult to observe by emission. This is why we chose to employ THG NSOM to investigate the spatial distribution of interchain species in MEH-PPV films.
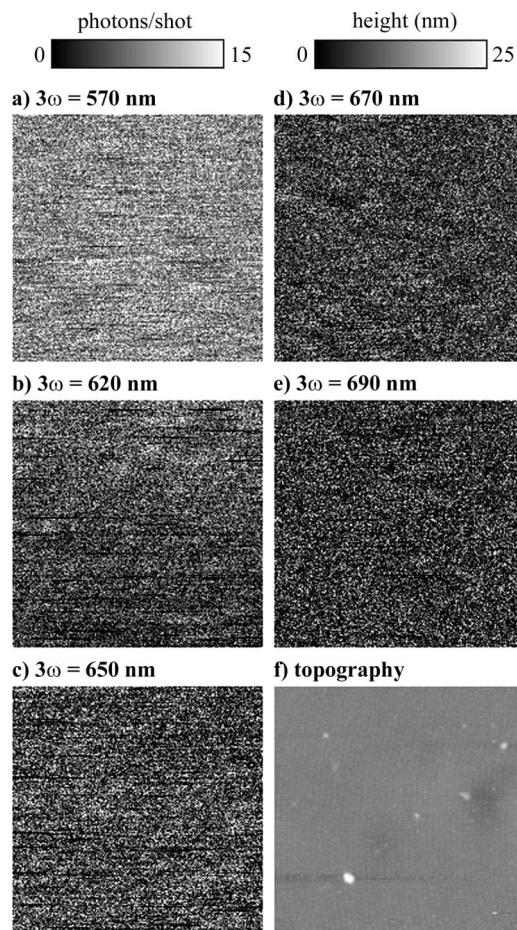
FIG. 2. THG NSOM images of as-cast MEH-PPV films. (a)–(e) THG NSOM images were produced at $3\omega = 570$, 620, 650, 670, and 690 nm, respectively, for the same $(8~\mu m)^2$ area shown topographically in (f) for an *as-cast* MEH-PPV film. Contrast is not observable in any of the images, including that in (a) in which the THG is resonant with the single-chain MEH-PPV absorption spectrum [cf. Fig. 4(b)].

FIG. 3. THG NSOM images of annealed MEH-PPV films. (a)–(e) THG NSOM images were produced at $3\omega = 570$, 620, 650, 670, and 690 nm, respectively, for the same $(8~\mu m)^2$ area shown topographically in (f) for a *thermally annealed* MEH-PPV film. In (a), when 3ω is resonant with single-chain species, higher THG signal levels are observed compared to the as-cast films studied in Fig. 2. While there is no contrast at $3\omega = 570$, contrast is observed in (b)–(d), a result we assign to resonance enhancement from a redshifted transition associated with spatially inhomogeneous aggregation domains. Contrast is not observable when 3ω becomes lower in energy than the lowest allowed transition frequency of the aggregates, as seen in (e).

B. Wavelength dependence of spatially resolved THG: Aggregation domains in annealed MEH-PPV films

Reproducible THG NSOM images with incident laser frequencies $3\omega = 570$, 620, 650, 670, and 690 nm are shown in Figs. 2(a)–2(e), respectively, from a typical $(8~\mu m)^2$ region of an MEH-PPV film spin-cast from chlorobenzene. The topography of this as-cast film, displayed in Fig. 2(f), shows small (~ 100 nm), circular bumps that we have argued previously to be due to the presence of entangled polymer chains in the solution from which the film is cast.[10] Our previous PL NSOM experiments showed that these features contain higher concentrations of emissive interchain species than the flat regions of the films.[12] The THG signal levels for the data in Fig. 2 are highest (~ 15 photons/shot) for the bluest wavelength in the image series [Fig. 2(a), $3\omega = 570$ nm], and decrease (to ~ 4 photons/shot) as the incident laser is tuned further to the red. No perceptible contrast is observable in any of the images, with the possible exception of some very faint features in Fig. 2(b) that do not appear to correlate with the topographical features on the surface of the film.

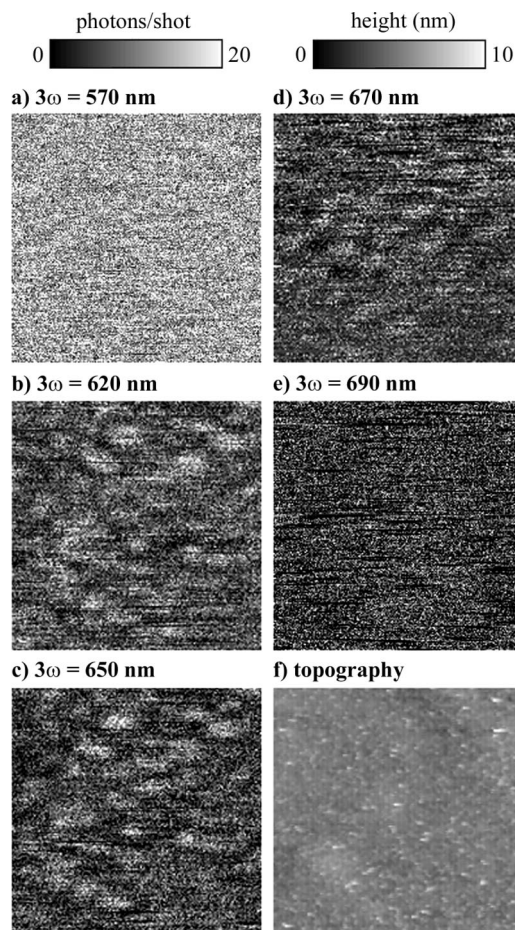Results from THG NSOM measurements performed on a thermally annealed MEH-PPV film are displayed in Figs. 3(a)–3(e) using the same set of wavelengths as for Fig. 2. Each of these images was produced for the same $(8~\mu m)^2$ area whose (featureless) topography is shown in Fig. 3(f). No contrast is observed in Fig. 3(a), the bluest wavelength in this image series ($3\omega = 570$ nm), despite the very strong THG signal levels (~ 20 photons/shot). Like the data presented in Fig. 2, the signal levels decrease as the laser is sequentially tuned further to the red [Figs. 3(b)–3(d)], in which $3\omega = 620$, 650, and 670 nm, respectively). In striking dissimilarity with the data in Fig. 2, however, many small, THG-efficient, prolate-shaped (aspect ratio of $\sim$ 3:1, length: width, width from 150 to 500 nm) features that have no topographical counterpart become observable at these redder wavelengths. The features in Figs. 3(b) and 3(c) appear to be nearly identical. The image contrast is reduced as the laser is tuned further to the red in Fig. 3(d) ($3\omega = 670$ nm), while the image in Fig. 3(e) ($3\omega = 690$ nm) appears almost completely featureless.

The high signal levels and lack of observable contrast in the THG NSOM images of both as-cast and annealed films when the third harmonic is tuned to 570 nm, as in Figs. 2(a) and 3(a), suggest resonance enhancement by a species that uniformly comprises the entire film. It is well known from photoluminescence excitation and absorption measurements that 570 nm is a wavelength that is coincident with the onset of the electronic resonance of single MEH-PPV chromophores.[40] Thus, the lack of THG contrast at this wavelength results because the entire film contains polymer chains that have an electronic resonance at this energy, independent of whether or not the chains are associated with interchain species.

Unlike the images collected at $3\omega = 570$ nm, there is strong contrast in the THG NSOM images of annealed films, [Figs. 3(b)–3(d) ($3\omega = 620$, 650, and 670 nm, respectively] that is lacking in the corresponding images of as-cast films in Fig. 2. This reveals that a significant alteration of the electronic structure and film homogeneity results from annealing. The sizes of the observed domains, which are larger than our optical spatial resolution of $\sim$100 nm,[51] indicates that annealing results in *localized* changes in the electronic structure of the polymer chains. Moreover, the fact that contrast is observed only in images in which the third harmonic is tuned to the red edge of the absorption spectrum suggests that a resonance enhancement contrast mechanism is operative: the bright regions in the image must contain species that have an electronic absorption at these red wavelengths, while no such species are present in the dark regions on the image. The loss of contrast in Fig. 3(e) ($3\omega = 690$ nm) is also consistent with a resonant enhancement mechanism as the source of contrast in Figs. 3(b)–3(d), because nonresonant effects would not exhibit such wavelength dependence. The fact that light is selectively absorbed between 620 and 670 nm in the bright regions indicates that there must be domains with increased ground-state π-electron delocalization, as typical single polymer chains do not absorb at wavelengths this red.

As mentioned above, there are two possible ways that annealing could lead to increased ground-state electron delocalization: by increasing the conjugation length of *single* conjugated polymer chains, or by the formation of *ground-state interchain* electronic species. An increase of electron delocalization in single-chain species, however, is unlikely to be the source of contrast in Figs. 3(b)–3(d) because the extent of delocalization along the polymer backbone is known to saturate well before a single chain could absorb this far to the red.[60] Moreover, if single-chain delocalization were the predominant effect upon annealing, we would have expected the thermal removal of kinks and other defects to result in a homogeneous spatial distribution of chains with differing conjugation lengths, rather than in distinct and isolated regions with increased conjugation. Finally, we know from our previous PL NSOM studies[12,64] that emissive interchain species are present in high concentrations in annealed MEH-PPV films. It is worth pointing out, however, that our previous studies could not ascertain whether or not the interchain emission resulted from ground-state aggregates. The red-shifted emission could have been generated by emissive excited-state interchain species or by interchain states popu-

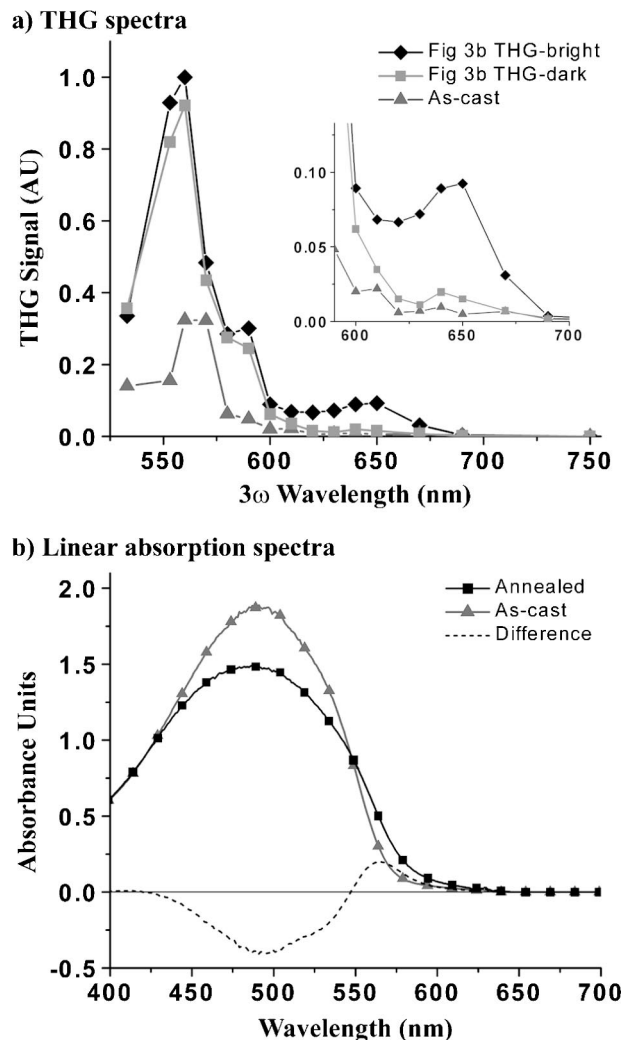## a) THG spectra

b) Linear absorption spectra

FIG. 4. Spatially resolved THG NSOM spectra. (a) Spectrally resolved THG efficiency measurements for three different regions of an annealed MEH-PPV film: diamonds show the spectrum from one of the bright regions in Figs. 3(b)–3(d); squares denote the spectrum for one of the dark regions in Figs. 3(b)–3(d), while triangles show the THG spectrum for a typical region of an as-cast film (Fig. 2). The spectrum collected from the bright region shows enhancement at lower energy that is not observed in the THG-dark regions of annealed films or in as-cast films (inset), suggestive of aggregate absorption. (b) Linear absorption spectra for annealed (squares) and as-cast (triangles) MEH-PPV films; the absorption onset shifts to the red upon annealing.

lated via energy transfer from the excitation of nearby single-chain chromophores;[72,73] the data here show that at least some of this emission arises from ground-state aggregates.

We can obtain more insight into the electronic structure of the red-absorbing species revealed in Figs. 3(b)–3(d) by studying the wavelength dependence of the THG efficiency. Figure 4(a) presents the spatially resolved wavelength dependence of the THG in the range of $3\omega = 533$ to 750 nm ($\omega = 1.60$ to 2.25 μm) for three characteristic MEH-PPV film regions: a typical region from an as-cast film, one of the THG-bright regions from an annealed film [cf. Fig. 3(b)], and one of the THG-dark regions from an annealed film.[74] The shapes of the spectra from $3\omega = 533$ to 600 nm for all three regions are similar, although the THG responses from the annealed film regions are approximately three times

stronger than that from the as-cast film. In all three spatial regions studied, the THG efficiency to the blue of $3\omega = 560$ nm, which is resonant with the main single-chain absorption band in each film, is decreased because the generated light is partially absorbed before detection (the films have very high optical densities at such wavelengths). The relative increase in THG efficiency for the annealed versus the as-cast films at these blue wavelengths may reflect an increase in the average conjugation length of single-chain chromophores upon annealing, as is also suggested by the absorption spectra shown in Fig. 4(b). The similarity of the THG efficiency for the two annealed film regions in this wavelength range also explains the lack of contrast observed in Fig. 3(a) ($3\omega = 570$ nm). As expected based on the high contrast seen in Figs. 3(b)–3(d), the efficiency of the THG-bright features in the annealed films shows a large enhancement in the region of $3\omega = 610$ to 670 nm relative to the other two regions. This red-enhanced THG verifies that the bright domains of Figs. 3(b)–3(d) represent distinct electronic species characterized by increased electron delocalization that occurs upon annealing. Based upon the red-enhanced THG and mesoscopic size of these features, we assign these regions to domains of ground-electronic-state interchain species: aggregation domains.

C. THG polarization dependence: The orientation of aggregation domains

One question raised by the existence of aggregation domains is whether or not the chains in such domains show any preferential alignment. This can be investigated by examining how the THG signal depends on the polarization of the incident laser. Results of THG NSOM studies conducted at $3\omega = 620$ nm using both p and s incident laser polarizations are shown in Fig. 5 for the same $(10\ \mu m)^2$ area of an annealed MEH-PPV film [the topography is not shown but is featureless, similar to Fig. 3(f)]. A similar number of high THG efficiency domains appear for both incident laser polarizations, and the bright domains seen with each polarization have a similar size, shape, and THG efficiency. In the analysis presented below [using the digitally filtered and combined images shown in Figs. 5(c) and 5(d)], we find that the domains observed with p and s are predominantly located in nonoverlapping spatial regions of the film: there are not many regions that produce strong THG for both incident polarizations. This result provides evidence that the aggregation domains observed in annealed MEH-PPV films consist of aligned polymer chains (orientation domains) that maximize π-electron overlap between the aromatic backbones.

The high polarization sensitivity of THG observed by Saito and co-workers[55] implies that there may be additional aggregation domains that we do not observe because they might be aligned with their main polarizability axis parallel to the propagation direction of the incident laser. Such domains would produce much less third harmonic than those that have a significant component of their main polarizability axis in the direction of the incident laser polarization. Spin-cast films of MEH-PPV have been shown to be birefringent because of a preference for chains to orient in the plane of the film, while the chain orientation in directions parallel to
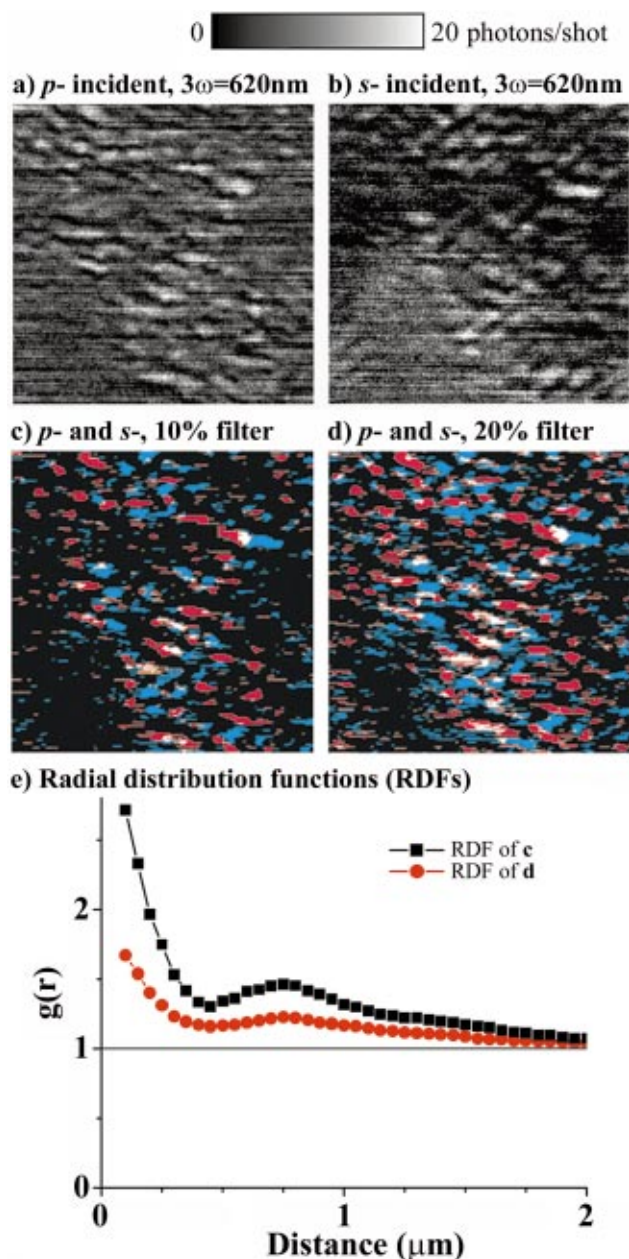

FIG. 5. (Color) Orientation of and correlation between aggregation domains. THG NSOM images produced at $3\omega = 620$ nm with (a) p [similar to Fig. 3(b)] and (b) s incident laser polarization, both for the same topographically featureless $(10\ \mu m)^2$ area of an annealed MEH-PPV film. These images were combined using a digital filtering scheme comparing pixel values to a threshold chosen to result in (c) 10% and (d) 20% total area coverage for each of the polarizations (see text for details). Pixels above threshold for p and s polarizations are shown in red and blue, respectively, while pixels above the threshold value for both polarizations are shown in white. Pixels below threshold are shown in black. Two-dimensional radial distribution function calculations for the images in (c) and (d) are shown as the squares and circles in (e), respectively. The RDFs clearly show a mathematical correlation between domains of increased THG efficiency.

the film is expected to be isotropic.[75] Similar measurements have not been performed for annealed films; thus, we must consider the possibility that partial or total rerandomization of this preferred in-plane orientation may occur during the annealing process, leading to domains with the chain backbones oriented normal to the plane of the film.

Now that we are aware of the existence of additional

aggregation domains that were not readily visible in the fixed-polarization scans of Fig. 3, we can use the information in Fig. 5 to learn more about the spatial distribution of aggregates in annealed films of MEH-PPV. To make use of the data in Fig. 5, we employed the following image processing scheme. The images were first digitally filtered by comparison of the value of each individual pixel to a threshold level. Pixels above the threshold value were assigned a value of 1 if more than three of their nearest-neighbor pixels were also above threshold (this criterion was used to account for the finite instrument spatial resolution). Pixels that did not meet this nearest-neighbor criterion or that were below the threshold were assigned a zero value. Next, the resulting digitally filtered images were combined using thresholds set to result in either 10% or 20% of the image areas being above threshold for each of the respective incident laser polarizations, as shown in Figs. 5(c) and 5(d), respectively. Two-dimensional radial distribution functions[76] (RDFs) calculated from the filtered and combined images are shown in Fig. 5(e). RDFs calculated using this same scheme without the described nearest-neighbor criterion were not significantly different from those presented in Fig. 5(e).

The purpose of this RDF analysis is to provide a quantitative measure of the interdomain structure that arises in films of MEH-PPV upon thermal annealing. Because this is a novel method of NSOM data interpretation, we have been careful to consider the pitfalls that might result from such an analysis. One concern involves applying a two-dimensional (2D) analysis to images that constitute a 2D projection of species that may exist at different 3D depths into the 200 nm thick films. However, even if the aggregation domains were actually 2D objects (rather than 3D objects) and were staggered at the top and bottom of the film thickness in an alternating pattern, the effect would only be to blur the RDF at short distances. This effect should be less significant than the blurring of the RDF that results from the circular averaging over the prolate shape of the domains in this case. A second concern is that NSOM measurements are thought to have an exponential dependence of the coupling of the optical signals into the near-field probe with sample–tip distance.[77–79] The THG signal levels for most of the aggregation domains we observe, however, appear to be similar. This implies that the distances over which most of the domains are separated from the tip are similar. The THG NSOM images show that the in-plane domain dimensions are $\sim 600 \times 200$ nm on average, which is significant with respect to the film thickness (~ 200 nm). Hence, it is likely that the aggregation domains span the entire thickness of the films, making a 2D analysis even more reasonable in this case.

With these caveats in mind, the 2D RDFs shown in Fig. 5(e) show three interesting features: a strong correlation of bright pixels with other bright pixels at short distances (≤ 400 nm), a second correlation distance near 750 nm, and loss of correlation at distances longer than ~ 1.5 μm. Such RDFs are characteristic of the structure of amorphous liquids.[76] The short-distance correlation reflects the circularly averaged diameter (~ 380 nm) of the prolate-shaped aggregation domains. A smaller, broader peak appears near 750 nm, indicating that there is an increased likelihood of domain

formation at this distance from another domain. At distances longer than ~ 1.5 μm, the domains exhibit lack of correlation: the $g(r)$ converges to 1. Between these two correlation peaks, the correlation function does not dip below 1, which is due to averaging circularly over the prolate shape of the domains.

Our interpretation of the features in the RDFs is that aggregate domains are limited in size by increasing steric frustration as the mesoscopic domains grow to ~ 380 nm (again, circularly averaged over the prolate domain shape). The asymmetric, branched solubilizing side groups of MEH-PPV were designed to prevent crystallization, making it increasingly difficult to pack the chains in an aligned fashion with increasing domain size. This frustration likely results in reduced overlap of the ground-state wave functions when the domains become too large, although we cannot rule out the possibility that the aggregation domains could be subsets of still larger orientation domains, as putatively observed with PM NSOM.[30]

We close this section by noting that the combined s and p incident polarization images shown in Figs. 5(c) and 5(d) resulted in 18% and 36% of the respective image areas being above threshold. Using either of the digital filters, we find that there is $<10\%$ overlap between the bright regions observed with different incident laser polarizations. This lack of a significant overlap between the images produced with different incident polarization confirms that a single polarizability component dominates the third-order response from the aggregated regions. This polarizability could result either from the $\alpha^{(3)}_{\zeta\zeta\zeta\zeta}$ component of the third-order susceptibility (oriented along the polymer backbone) for individual polymer chains, or possibly from a large interchain polarizability that would be perpendicular to $\alpha^{(3)}_{\zeta\zeta\zeta\zeta}$. We are considering further experiments to elucidate the directional nature of the interchain polarizability responsible for the observed THG contrast.

D. Aggregation domains in as-cast films: Aggregation in solution

While the data in Figs. 2 and 3 imply that thermal annealing is necessary to produce ground-state interchain species in conjugated polymers, there is THG NSOM evidence that a limited number of aggregation domains form in as-cast MEH-PPV films. Figure 6 demonstrates that one of the topographical bumps on the surface of a MEH-PPV film cast from chlorobenzene shows increased THG efficiency when imaged at $3\omega = 620$ nm. We emphasize that this result is not typical for as-cast films; we see such aggregation signatures in as-cast films only infrequently.

The observation of aggregation domains in as-cast films, though rare, is significant because it verifies that aggregates can form in solution (without the increased thermal activation provided by annealing) and are able to survive the casting process to produce as-cast conjugated polymer films that are spatially inhomogeneous. We have already argued from PL NSOM studies that the interchain species that form in solution survive the spin-casting process to produce topo-
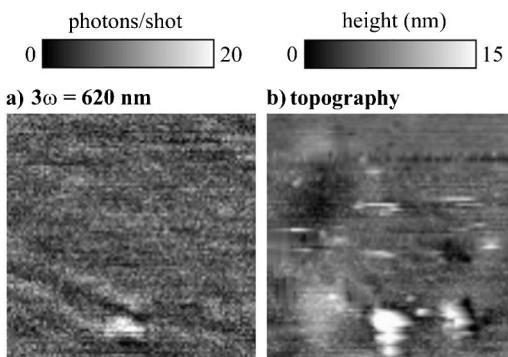
photons/shot   height (nm)

0 [====] 20   0 [====] 15

a) 3ω = 620 nm   **b) topography**

FIG. 6. Aggregate domains in as-cast films. (a) THG NSOM image produced at $3\omega = 620$ nm for a $(5 \ \mu m)^2$ area of an as-cast film shown topographically in (b). High THG signal levels are observed at a position that corresponds to a topographical bump in the lower center of the area studied. Increased THG signal levels extend beyond the location of the topographic feature, which we attribute to the interchain species extending further into the film. We observe such THG features only rarely in as-cast films, suggesting that interchain PL observed in previous studies (Ref. 12) is due mostly to excited-state-only interchain species such as excimers rather than to ground-state aggregates.

graphical bumps on the surface of MEH-PPV films that are characterized by a red-shifted interchain emission.[12] The fact that the THG signatures of aggregation are only infrequently correlated with morphological bumps in as-cast films indicates that the interchain species studied in our previous PL NSOM work are predominantly excited-state-only interchain species, such as excimers or polaron pairs. This result has implications for the way in which MEH-PPV chains pack in films. We expect that overlap of ground-state wave functions will occur only when conjugated polymer chains approach each other very closely, whereas excited-state wave functions, which extend further from the polymer backbone, are likely to overlap at larger backbone separations. Thus, our observations suggest that because it is difficult to pack adjacent chromophores closely together, ground-state wave function delocalization is not a significant component of the electronic structure of as-cast MEH-PPV films. Ground-state delocalization does become important, however, when the chains can pack more closely together upon thermal annealing.

IV. CONCLUSIONS

Using THG NSOM, we have observed many (18–36 % by area) small ($\sim 600 \times \sim 200$ nm) domains with increased ground-state π-electron delocalization in thermally annealed films of MEH-PPV. These aggregation domains were observed when the third harmonic was tuned to wavelengths redder than the onset of absorption of single MEH-PPV chains. Increased ground-state delocalization in these domains was characterized by measuring the THG efficiency of different film regions as a function of wavelength. Polarization-dependent THG NSOM images revealed that the domains consist of oriented polymer chains that must be packed tightly in order to account for the observed degree of ground-state wave function delocalization. The domains form in abundance upon thermal annealing, but we do infrequently observe aggregation domains in as-cast MEH-PPV

films that are associated with topographical bumps on the film surface. All of these results verify that ground-state aggregation is highly dependent on the details (such as choice of casting solvent or annealing) of the processing of polymer solutions into films.

We speculated that the mesoscopic scale of the aggregation domains could result from a nucleation and growth mechanism during the thermal annealing process. When two proximal polymer chain segments become sufficiently straight, they can pack together very closely and form an interchain species; the straightened polymer segments will thus become more likely to stay straight rather than to fluctuate. As other polymer chains fluctuate through conformational space, adjacent instantaneously straight segments will tend to pack together with the interchain "seed" that is not significantly fluctuating in shape. This process will continue to make the interchain moiety grow in size until steric strain and defects in the packing of the individual polymer chains reduce the thermodynamic driving force for aggregation and halt the growth of the domain.

We close by comparing the above results to recent work in which we have detected solvatochromic domains in annealed films of MEH-PPV using PL NSOM.[64] In this solvatochromic study, liquids of high polarity were placed in contact with the surfaces of annealed MEH-PPV films and spatially resolved PL spectra were acquired. While the PL collected from the films was homogeneous in the absence of applied liquids, we found solvatochromic domains characterized by a redshifted PL when the liquid was in contact with the film. The solvatochromic domains were both substantially larger ($\sim 1 \ \mu m$ diameter) and rarer in occurrence (covering $\leqslant 5\%$ of the total film area) than the aggregation domains observed here using THG NSOM. We note that the experimental techniques used in these two studies probe different electronic properties of the films as well as sample different depths of field. THG NSOM is a probe of the absorptive sample properties whereas PL solvatochromism measures emissive sample properties; thus the PL experiments cannot discriminate against the possibility of transfer of the initial excitation from one type of species to another due to energy funneling processes. Rothberg and co-workers have pointed out that MEH-PPV aggregates have very low emission quantum yields at room temperature, which indicates that the features observed in this THG work are not likely to be the same as those in the emission solvatochromism measurements.[13] To verify this, we have conducted extensive PL NSOM imaging studies (using cw excitation at 532 nm) of annealed MEH-PPV films and have not observed optical contrast or features like those presented in Figs. 3(b)–3(d). The depth of field of our solvatochromic NSOM experiments, conducted in oblique collection mode, is also quite different from the present THG study. The solvatochromically shifted emission is collected only from those chromophores localized within a few nanometers of the surface for three reasons: (1) the exponentially decreasing coupling of optical signals to the tip with distance from the tip,[77–82] (2) the high optical density of the film at the excitation wavelength (532 nm), which produces a selective excitation of the surface chromophores, and (3) the fact that

only chromophores near the surface are sensitive to the presence of the highly polar liquid. The present THG NSOM experiments, in contrast, exhibit a much larger depth of field. This is because (1) the sample is transparent at the wavelength of the incident laser; and (2) resonance enhancement of THG signals can increase signal levels by orders of magnitude[47] such that for nonlinear sources a larger depth into the sample may be observable despite the exponential coupling of optical signals to the tip. Thus, we believe that these two different NSOM measurements probe distinct, though coexisting species in annealed films of MEH-PPV.

Collectively, our results suggest that the ground-state electronic properties of conjugated polymer films become highly inhomogeneous upon annealing. As-cast films contain topographical features that are associated primarily with weakly emissive, excited-state interchain species and occasionally with weakly absorptive ground-state interchain species; the degree of interchain species formation depends sensitively on the way the film was processed from solution. Annealed MEH-PPV films have an even more complex structure, containing large orientation domains that are also associated with ground-state aggregation, and several types of domains of emissive excited-state interchain species that can be detected via solvatochromism NSOM. Given the importance of interchain species in charge transport, in luminescence efficiency (including energy funneling), and potentially in device degradation, it is clear that a more detailed knowledge of how conjugated polymer chains interact is essential to make the best use of these materials in optoelectronic devices.

[1] A. J. Lovinger and L. J. Rothberg, J. Mater. Res. **11**, 1581 (1996).
[2] R. H. Friend, R. W. Gymer, A. B. Holmes, *et al.*, Nature (London) **397**, 121 (1999).
[3] J. H. Burroughes, D. D. C. Bradley, A. R. Brown, R. N. Marks, K. Mackay, R. H. Friend, P. L. Burns, and A. B. Holmes, Nature (London) **347**, 539 (1990).
[4] G. Gustafsson, Y. Cao, G. M. Treacy, F. Klavetter, N. Colaneri, and A. J. Heeger, Nature (London) **357**, 477 (1992).
[5] M. Granstrom, K. Petritsch, A. C. Arias, A. Lux, M. R. Andersson, and R. H. Friend, Nature (London) **395**, 257 (1998).
[6] N. S. Sariciftci, L. Smilowitz, A. J. Heeger, and F. Wudl, Science **258**, 1474 (1992).
[7] T. R. Hebner, C. C. Wu, D. Marcy, M. H. Lu, and J. C. Sturm, Appl. Phys. Lett. **72**, 519 (1998).
[8] J. Bharathan and Y. Yang, Appl. Phys. Lett. **72**, 2660 (1998).
[9] T. Q. Nguyen, R. C. Kwong, M. E. Thompson, and B. J. Schwartz, Appl. Phys. Lett. **76**, 2454 (2000).
[10] T. Q. Nguyen, I. B. Martini, J. Liu, and B. J. Schwartz, J. Phys. Chem. B **104**, 237 (2000).
[11] T. Q. Nguyen, R. C. Kwong, M. E. Thompson, and B. J. Schwartz, Synth. Met. **119**, 523 (2001).
[12] T. Q. Nguyen, B. J. Schwartz, R. D. Schaller, J. C. Johnson, L. F. Lee, L. H. Haber, and R. J. Saykally, J. Phys. Chem. B **105**, 5153 (2001).
[13] R. Jakubiak, L. J. Rothberg, W. Wan, and B. R. Hsieh, Synth. Met. **101**, 230 (1999).
[14] P. Wang, C. J. Collison, and L. J. Rothberg, J. Photochem. Photobiol., A **144**, 63 (2001).
[15] C. J. Collison, L. J. Rothberg, V. Treemaneekarn, and Y. Li, Macromolecules **34**, 2346 (2001).
[16] T. G. Bjorklund, S. H. Lim, and C. J. Bardeen, J. Phys. Chem. B **105**, 11970 (2001).
[17] E. M. Conwell, Phys. Rev. B **57**, 14200 (1998).
[18] S. A. Jenekhe and J. A. Osaheni, Science **265**, 765 (1994).
[19] T. Huser and M. Yan, J. Photochem. Photobiol., A **144**, 43 (2001).
[20] T. Q. Nguyen, R. Y. Yee, and B. J. Schwartz, J. Photochem. Photobiol., A **144**, 21 (2001).
[21] C. Y. Yang, F. Hide, M. A. DiazGarcia, A. J. Heeger, and Y. Cao, Polymer **39**, 2299 (1998).
[22] J. I. Lee, G. Klaerner, and R. D. Miller, Chem. Mater. **11**, 1083 (1999).
[23] T. W. Lee and O. O. Park, Appl. Phys. Lett. **77**, 3334 (2000).
[24] T. W. Lee, O. O. Park, L. M. Do, T. Y. Zyung, T. Ahn, and H. K. Shim, J. Appl. Phys. **90**, 2128 (2001).
[25] T. W. Lee and O. O. Park, Adv. Mater. **12**, 801 (2000).
[26] J. W. Blatchford, T. L. Gustafson, A. J. Epstein *et al.*, Phys. Rev. B **54**, R3683 (1996).
[27] J. W. Blatchford, S. W. Jessen, L. B. Lin, T. L. Gustafson, D. K. Fu, H. L. Wang, T. M. Swager, A. G. Macdiarmid, and A. J. Epstein, Phys. Rev. B **54**, 9180 (1996).
[28] J. A. Teetsov and D. A. Vanden Bout, J. Am. Chem. Soc. **123**, 3605 (2001).
[29] J. Teetsov and D. A. Vanden Bout, Langmuir **18**, 897 (2002).
[30] C. H. Tan, A. R. Inigo, J. H. Hsu, W. Fann, and P. K. Wei, J. Phys. Chem. Solids **62**, 1643 (2001).
[31] P. K. Wei, Y. F. Lin, W. Fann, Y. Z. Lee, and S. A. Chen, Phys. Rev. B **63**, 045417 (2001)
[32] M. Yan, L. J. Rothberg, E. W. Kwock, and T. M. Miller, Phys. Rev. Lett. **75**, 1992 (1995).
[33] J. A. DeAro, K. D. Weston, S. K. Buratto, and U. Lemmer, Chem. Phys. Lett. **277**, 532 (1997).
[34] J. A. DeAro, U. Lemmer, D. Moses, and S. K. Buratto, Synth. Met. **101**, 300 (1999).
[35] J. D. McNeill, D. B. O'Connor, and P. F. Barbara, J. Chem. Phys. **112**, 7811 (2000).
[36] N. C. Greenham, I. D. W. Samuel, G. R. Hayes, R. T. Phillips, Y. A. R. R. Kessener, S. C. Moratti, A. B. Holmes, and R. H. Friend, Chem. Phys. Lett. **241**, 89 (1995).
[37] I. D. W. Samuel, G. Rumbles, C. J. Collison, R. H. Friend, S. C. Moratti, and A. B. Holmes, Synth. Met. **84**, 497 (1997).
[38] A. Boudrioua, P. A. Hobson, B. Matterson, I. D. W. Samuel, and W. L. Barnes, Synth. Met. **111**, 545 (2000).
[39] J. M. Lupton, I. D. W. Samuel, R. Beavington, M. J. Frampton, P. L. Burn, and H. Bassler, Phys. Rev. B **63**, 155206 (2001).
[40] T. Q. Nguyen, V. Doan, and B. J. Schwartz, J. Chem. Phys. **110**, 4068 (1999).
[41] U. Lemmer, S. Heun, R. F. Mahrt, U. Scherf, M. Hopmeier, U. Siegner, E. O. Gobel, K. Mullen, and H. Bassler, Chem. Phys. Lett. **240**, 373 (1995).
[42] T. Pauck, R. Hennig, M. Perner *et al.*, Chem. Phys. Lett. **244**, 171 (1995).
[43] R. F. Mahrt, T. Pauck, U. Lemmer *et al.*, Phys. Rev. B **54**, 1759 (1996).
[44] M. Yan, L. J. Rothberg, F. Papadimitrakopoulos, M. E. Galvin, and T. M. Miller, Phys. Rev. Lett. **72**, 1104 (1994).
[45] B. Kraabel, V. I. Klimov, R. Kohlman, S. Xu, H. L. Wang, and D. W. McBranch, Phys. Rev. B **61**, 8501 (2000).
[46] D. Beljonne, J. Cornil, H. Sirringhaus, P. J. Brown, M. Shkunov, R. H. Friend, and J. L. Bredas, Adv. Funct. Mater. **11**, 229 (2001).
[47] Y. R. Shen, *The Principles of Nonlinear Optics* (Wiley, New York, 1984).
[48] R. W. Boyd, *Nonlinear Optics* (Academic Press, Boston, 1992).
[49] We note that there is a dependence of THG efficiency on the excited state lifetime, Γ^{1}, as shown explicitly in Eq. (3).
[50] R. D. Schaller, J. C. Johnson, and R. J. Saykally, Anal. Chem. **72**, 5361 (2000).
[51] R. D. Schaller, J. C. Johnson, K. R. Wilson, L. F. Lee, L. H. Haber, and R. J. Saykally, J. Phys. Chem. B **106**, 5143 (2002).

[52] R. D. Schaller, C. Roth, D. H. Raulet, and R. J. Saykally, J. Phys. Chem. B **104**, 5217 (2000).

[53] R. D. Schaller and R. J. Saykally, Langmuir **17**, 2055 (2001).

[54] R. D. Schaller, J. Ziegelbauer, L. F. Lee, L. H. Haber, and R. J. Saykally, J. Phys. Chem. B (in press).

[55] K. Kamiyama, M. Era, T. Tsutsui, and S. Saito, Jpn. J. Appl. Phys., Part 2 **29**, L840 (1990).

[56] G. Berkovic, R. Superfine, P. Guyot-Sionnest, Y. R. Shen, and P. N. Prasad, J. Opt. Soc. Am. B **5**, 668 (1988).

[57] F. Kajzar and J. Messier, Thin Solid Films **132**, 11 (1985).

[58] A. Mathy, K. Ueberhofen, R. Schenk, H. Gregorius, R. Garay, K. Mullen, and C. Bubeck, Phys. Rev. B **53**, 4367 (1996).

[59] C. J. Yang, S. A. Jenekhe, J. S. Meth, and H. Vanherzeele, Ind. Eng. Chem. Res. **38**, 1759 (1999).

[60] I. Ledoux, I. D. W. Samuel, J. Zyss, S. N. Yaliraki, F. J. Schattenmann, R. R. Schrock, and R. J. Silbey, Chem. Phys. **245**, 1 (1999).

[61] T. Huser and M. Yan, Synth. Met. **116**, 333 (2001).

[62] L. F. Lee, R. D. Schaller, L. H. Haber, and R. J. Saykally, Anal. Chem. **73**, 5015 (2001).

[63] J. C. Johnson, H. Yan, R. D. Schaller, P. B. Petersen, P. Yang, and R. J. Saykally, Nano Lett. **2**, 279 (2002).

[64] R. D. Schaller, L. F. Lee, J. C. Johnson, L. H. Haber, R. J. Saykally, J. Vieceli, I. Benjamin, T.-Q. Nguyen, and B. J. Schwartz, J. Phys. Chem. B (in press).

[65] H. Antoniadis, L. J. Rothberg, F. Papadimitrakopoulos, M. Yan, M. E. Galvin, and M. A. Abkowitz, Phys. Rev. B **50**, 14911 (1994).

[66] M. Zheng, G. L. Bai, and D. B. Zhu, J. Photochem. Photobiol., A **116**, 143 (1998).

[67] D. H. Hu, J. Yu, K. Wong, B. Bagchi, P. J. Rossky, and P. F. Barbara, Nature (London) **405**, 1030 (2000).

[68] J. Yu, D. H. Hu, and P. F. Barbara, Science **289**, 1327 (2000).

[69] J. A. DeAro, D. Moses, and S. K. Buratto, Appl. Phys. Lett. **75**, 3814 (1999).

[70] G. M. Credo, G. M. Lowman, J. A. DeAro, P. J. Carson, D. L. Winn, and S. K. Buratto, J. Chem. Phys. **112**, 7864 (2000).

[71] J. D. McNeill, D. B. O'Connor, D. M. Adams, P. F. Barbara, and S. B. Kammer, J. Phys. Chem. B **105**, 76 (2001).

[72] T. Q. Nguyen, J. J. Wu, V. Doan, B. J. Schwartz, and S. H. Tolbert, Science **288**, 652 (2000).

[73] T. Q. Nguyen, J. Wu, S. H. Tolbert, and B. J. Schwartz, Adv. Mater. **13**, 609 (2001).

[74] THG efficiency was also measured in this same wavelength range for a sample of ZnSe, which does not exhibit resonances in this spectral region (band gap ~2.8 eV at 298 K). This measurement was performed to check for systematic artifacts in the wavelength-dependent THG efficiency scans. These scans resulted in a featureless, slightly negatively sloping (stronger THG at bluer wavelengths), straight line as is expected indicating a lack of artifacts.

[75] D. McBranch, I. H. Campbell, D. L. Smith, and J. P. Ferraris, Appl. Phys. Lett. **66**, 1175 (1995).

[76] D. Chandler, *Introduction to Modern Statistical Mechanics* (Oxford University Press, New York, 1987).

[77] M. A. Paesler and P. J. Moyer, *Near-Field Optics: Theory, Instrumentation, and Applications* (Wiley, New York, 1996).

[78] E. Betzig and J. K. Trautman, Science **257**, 189 (1992).

[79] R. C. Dunn, Chem. Rev. **99**, 2891 (1999).

[80] B. Hecht, B. Sick, U. P. Wild, V. Deckert, R. Zenobi, O. J. F. Martin, and D. W. Pohl, J. Chem. Phys. **112**, 7761 (2000).

[81] C. Girard, C. Joachim, and S. Gauthier, Rep. Prog. Phys. **63**, 893 (2000).

[82] R. E. Larsen and H. Metiu, J. Chem. Phys. **114**, 6851 (2001).